
Article:
Morales Corona, J.J., Sedransk Campbell, K. and Fennell, P.S. (2023) Enhancement of iron-based oxygen carriers through alloying with tungsten oxide for chemical looping applications including water splitting. Greenhouse Gases: Science and Technology, 13 (4). pp. 565-574. ISSN 2152-3878

https://doi.org/10.1002/ghg.2221

Original Article

GREENHOUSE GASES SCIENCE AND TECHNOLOGY

Enhancement of iron-based oxygen carriers through alloying with tungsten oxide for chemical looping applications including water splitting

Jose Juan Morales Corona, Department of Chemical Engineering, Imperial College London, London, UK
Kyra Sedransk Campbell, Department of Chemical Engineering, Imperial College London, London, UK and Department of Chemical and Biological Engineering, The University of Sheffield, Sheffield, UK
Paul S. Fennell, Department of Chemical Engineering, Imperial College London, London, UK

Abstract: Chemical looping applications offer a variety of options to decarbonise different industrial sectors, such as iron and steel and hydrogen production. Chemical looping with water splitting (CLWS) is a chemical looping technology, which produces H_2 while simultaneously capturing CO_2. The selection of oxygen carriers (OCs) available to be used in CLWS is finite, due to the thermodynamic limitations of the oxidation with steam for different materials at the relevant process temperatures. Iron-based materials are one of the most widely studied options for chemical looping combustion (CLC), touted for their relative abundance and low cost; likewise, for CLWS, iron is the most promising option. However, when the reduction of iron oxide (Fe_2O_3) is extended to wüstite (FeO) and iron (Fe), agglomeration and sintering problems are the main challenge for fluidisation. This work presents iron and tungsten mixed oxides as the OCs for a family of chemical looping applications. The OCs were produced via co-precipitation; performance assessment was conducted in a thermogravimetric analyser and a lab-scale fluidised bed reactor over continuous redox cycles. The use of tungsten combined with iron results in a solid solution of tungsten within the Fe_2O_3 matrix that produced a more mechanically stable material during operation, which performed well during multiple redox cycles with no apparent decrease in the oxygen transport capacity and showed no apparent agglomeration. Furthermore, materials containing tungsten showed a resistance to carbon deposition, whereas the reference Fe_2O_3 showed peaks of CO and CO_2 during the oxidation period, thus indicating carbon deposition.

Keywords: CO_2 capture; chemical looping combustion; iron oxide; mixed oxides

Correspondence to: Department of Chemical Engineering, Imperial College London, SW7 2AZ, UK.
Email: p.fennell@imperial.ac.uk
Received January 30, 2023; revised April 28, 2023; accepted May 4, 2023
Published online at Wiley Online Library (wileyonlinelibrary.com). DOI: 10.1002/ghg.2221

Introduction

Global carbon dioxide emissions from fossil fuels combustion are the main contribution causing global warming. To achieve the global reduction targets in the near term, carbon capture and storage (CCS) technologies need to be placed to capture CO_2 from industry, which is the largest emitting sector of this greenhouse gas, with over 40% of the global emissions in 2019 (when heat and electricity emissions are allocated to final sectors).[1]

Chemical looping combustion (CLC) is part of the CCS technologies portfolio, in which redox reactions of metal oxides are used to transfer oxygen from the air to the fuel for combustion processes. Since direct contact between the fuel and air is avoided, a concentrated CO_2 stream without combustion impurities is produced, which then can be separated (through steam condensation), transported and stored.[2] The choice of metal oxide to be used as oxygen carrier (OC) depends on the CLC process, but mainly these materials need to maintain a high reactivity and a constant oxygen transport capacity (Ro) and remain both mechanically and chemically stable over extended periods of time.

Hydrogen production is achieved mainly via steam methane reforming (SMR), and accounts for around 3% of the global CO_2 emissions from the industry sector.[3] Chemical looping with water splitting (CLWS) is a CLC variant used for H_2 production, which is a promising option to reduce emissions while producing high purity H_2.[4] The most common configuration for CLWS is a three-reactor system, where a third reactor (steam reactor) is added to the standard CLC configuration (fuel and air reactors) (Fig. 1).[5]

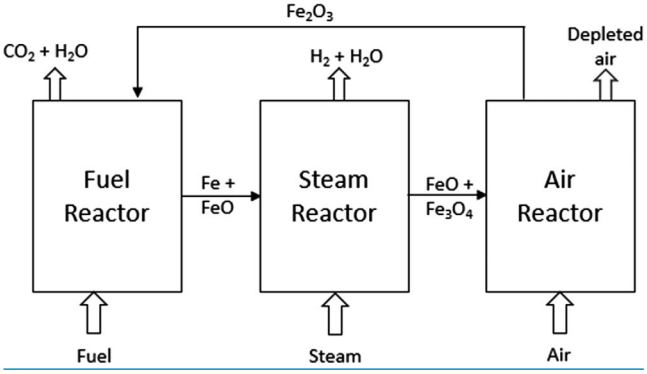

Figure 1. Chemical looping with water splitting process, where the oxide system of $Fe_2O_3/Fe_3O_4/FeO/Fe$ is used as oxygen carrier.

Thermodynamic limitations of the redox pairs that can be used for CLWS limit the options to just a few choices: Fe, W and Ce oxides.[6]

Fe-based oxygen carriers for CLC have been widely studied and represent an advantage when compared to the other options for CLWS due to its abundance, low cost and being environmental benign.[7,8] For most CLC applications, Fe-based oxygen carriers have been used in conditions to restrict the reduction of Fe_2O_3 to Fe_3O_4. Further reduction to FeO and Fe represent slower reaction kinetics and lower fuel combustion efficiencies when compared to reduction to only Fe_3O_4.[9,10] These limitations are due to the severe chemical and mechanical stresses to which the material is subjected, leading to an increased reactive/thermal sintering, which reduces the available reactive surface area.

In this work we present a new iron-tungsten mixed oxide for extended reduction in CLC as a first step towards its use in CLWS to produce hydrogen. We compare the performance of this new material with two different Fe_2O_3 sample materials that serve as a reference to quantify the improvements.

Experimental

Material synthesis

Synthesis of oxygen carriers via co-precipitation

The oxygen carriers were synthesised using an automated rig for co-precipitation, detailed elsewhere.[11] For the iron-tungsten (Fe-W) mixed oxide (to avoid confusion, the material was synthesized as a mixed oxide, which we believe then partially alloyed at reaction temperatures), two solutions were prepared for the synthesis: (1) $Fe(NO_3)_3.9H_2O$ and $Na_2WO_4.2H_2O$ were dissolved in deionised water (DI water) to obtain a 250 ml solution with a total ion concentration of 1 M (with a molar Fe-W ratio of 0.95:0.05 and 0.98:0.02) and (2) a 1 M solution of NaOH to regulate the pH.

The rig controlled the flow rates of the two solutions to maintain a constant pH value of 12 ± 0.1 during the co-precipitation under constant stirring. After addition of solution 1 was completed, the stirring was stopped, and the mixture was aged for 1 h. The precipitate was then washed, by adding DI water, followed by centrifugation at 3000 rpm for 5 min to separate out the phases. The washing process was repeated until the measured conductivity was $\sigma < 100\ \mu S$. The precipitate was then dried overnight at 60°C and calcined for 6 h

Table 1. Summary of oxygen carriers prepared for this study.

Sample name	Tungsten content (mol%)	Preparation method
FeW-5-CP	5	Co-precipitation
FeW-2-CP	2	Co-precipitation
Fe_2O_3-MM	-	Mechanically mixing
Fe_2O_3-CP	-	Co-precipitation

at 900°C in air (2 L•min^{-1}) using a horizontal tube furnace with a heating rate of 15°C•min^{-1}.

Two reference samples of Fe_2O_3 were prepared for comparison. The first sample was prepared following the same co-precipitation procedure but without the addition of $Na_2WO_4.2H_2O$.

Synthesis of oxygen carriers via mechanical mixing

A second reference sample was prepared from a commercially available material. A batch of mechanically mixed (MM) oxygen carriers was prepared by mixing 0.2 mol of Fe_2O_3 (powder <5 μm, > 96% from Sigma-Aldrich) with 30 ml of DI water. The slurry was loaded into a planetary ball mill (PM-400, RETSCH) and was milled together with steel balls for 6 h at 250 rpm. The sample was dried and calcined under the same conditions as the co-precipitated materials.

A summary and nomenclature of the samples prepared for this study is presented in Table 1.

Oxygen carrier characterization and testing

Powder X-ray diffraction (XRD) analysis was carried out in a D2 Phaser (Bruker) using Cu-Kα radiation with $\lambda = 1.541$ Å. Scanning electron microscopy (SEM) in a JEOL JSM 6010LA at 20 kV was used to observe the surface morphology of the fresh and reacted particles. The crushing strength of the oxygen carriers was measured using a 50 N force gauge (Mark-10). Nitrogen adsorption analysis was done using a TriStar 3000 (Micromeritics) sorption analyser with N_2 at 77K, to determine the surface areas (BET), pore size distributions and volume of the micro and mesopores (size range up to~200 nm - BJH). Mercury intrusion porosimetry (MIP) was carried out using an AutoPore IV 9500 (Micromeritics) porosimeter to determine the pore volume in the region outside of the resolution of N_2 adsorption, between 10 nm and 10 μm. Helium pycnometry was carried out using an AccuPyc II 1340 (Micromeritics) pycnometer to determine the skeletal density of the oxygen carriers.

A thermo-gravimetric analyser (TGA) model Q5000 (TA Instruments) was used to analyse the materials. Isothermal redox cycling was performed to evaluate the conversion and redox capability of the oxygen carriers (particle size range of 150–300 μm). A platinum crucible ($h = 1.5$ mm, $d = 9.8$ mm) was used to hold a layer of OC (5 $\pm$ 0.3 mg) in each experimental run. The total gas flow rate used in all experiments was kept constant at a value of 200 ml•min^{-1} (SATP). A purge stage of N_2 was used to separate each reduction and oxidation stage and thus avoid gas mixing in the reaction chamber. The observed rate of reaction (in mol•g^{-1}•s^{-1}), was calculated from the weight loss (for the reduction) and weight gain (for the oxidation) periods of the experiment. The weight profiles obtained from the TGA were differentiated with respect to the time and divided through the initial mass of the fully oxidised sample. Redox-cycling experiments with a higher sample mass of OCs in the TGA (40 mg) was carried out to measure the crushing strength and perform XRD-analysis of the cycled particles. The experiments with a higher sample mass were performed with increased cycle times, for both the reduction and oxidation periods, to match the experimentally obtained Ro of the experiments with the low sample mass.

Tests were complemented with redox cycling experiments performed in a lab-scale fluidised bed reactor (FBR).[12] An inert experiment was carried out initially with 40 g of quartz sand (425–500 μm). Then, 0.5 g of OCs in the particle size range of 300–425 μm was added to the bed and the cycling experiment was run with the bed containing the sample. The change of gas concentration was measured continuously during the experiment and the data was deconvoluted to account for gas mixing and response time of the gas analyser following a method described elsewhere.[13]

Results and discussion

Characterisation results

Tungsten addition into the materials increased the porosity measured using both techniques. The BET surface area increased for the FeW-5-CP and FeW-2-CP samples to values of 3.77 and 3.39 m^2•g^{-1}

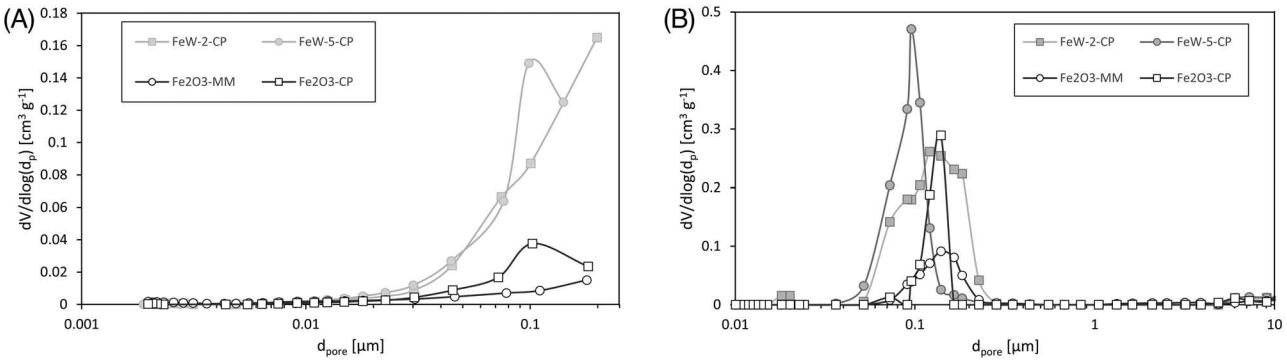

Figure 2. Pore size distributions determined by (A) BJH N_2-adsorption analysis, and (B) MIP analysis on the entire pore size range of the fresh oxygen carrier particles for all the samples prepared in this study.

Table 2. Summary of MIP, N_2 adsorption and He pycnometry measurements to determine the pore size distributions and porosity for the different OCs prepared for this work.

	FeW-5-CP	FeW-2-CP	Fe_2O_3-MM	Fe_2O_3-CP
BET surface area [$m^2 \bullet g^{-1}$]	3.77	3.39	2.48	1.94
Cumulative pore vol. (BJH) [$cm^3 \bullet g^{-1}$]	0.065	0.045	0.009	0.022
Cumulative pore vol. (MIP) [$cm^3 \bullet g^{-1}$]	0.089	0.092	0.030	0.042
Average d_p (4 V/A) (MIP) [nm]	466	420	1,200	760
Skeletal density (He pyc.) [$g \bullet cm^{-3}$]	5.07	5.24	5.05	5.00
Porosity (MIP)	0.628	0.634	0.485	0.458

respectively, when compared to the reference samples, with values of 2.48 and 1.94 $m^2 \bullet g^{-1}$ for the Fe_2O_3-MM and Fe_2O_3-CP samples, respectively. The total volume of pores measured for the reference samples was smaller than that for the Fe-W mixed oxide samples. In addition, the measured skeletal density by He pycnometry showed a slight increase with the addition of W in the analysed samples (size range 300–425 μm).

The total porosity of the materials measured by MIP showed an increase by the W addition into the material to values of around 60%, when compared to the Fe_2O_3 reference samples (below 50%). The pore size distributions of the OCs were found to shift towards smaller pore diameters (Fig. 2B).

Pore size distributions determined by N_2 adsorption and MIP are presented in (Fig. 2A and B), respectively. The results of the porosity measurements are summarised in Table 2.

Thermogravimetric screening and testing of the redox capability of the OCs

The redox capability of the oxygen carrier samples was tested in the TGA. A comparison between the two Fe_2O_3 reference samples and the co-precipitated Fe-W oxygen carriers was carried out over 50 redox-cycles at 850°C under a reducing environment of 15 vol% CO + N_2 for 10 min and oxidised in 4 vol% O_2 + N_2 for 20 min. These preliminary experiments were conducted with CO to avoid the complexity of operating a TGA with steam addition. The O_2 concentration on the oxidation step was chosen to be low to avoid any localised hot spots due to temperature gradients in the material since the oxidation of Fe-based materials is highly exothermic.

Reference Fe_2O_3 samples

The reactivity of the Fe_2O_3-MM and Fe_2O_3-CP samples was screened in the TGA to serve as reference and be able to compare the improvements made by adding W to the materials. The results of these experiments are presented in Fig. 3.

An analysis of the relative weight change and the Ro of both samples, (Fig. 3A and C) for the Fe_2O_3-MM and (Fig. 3B and D) for Fe_2O_3 co-precipitated, shows that all the lattice oxygen available for reaction was used on the first reduction cycle for both materials. Despite this, the oxidation does not recover back to a

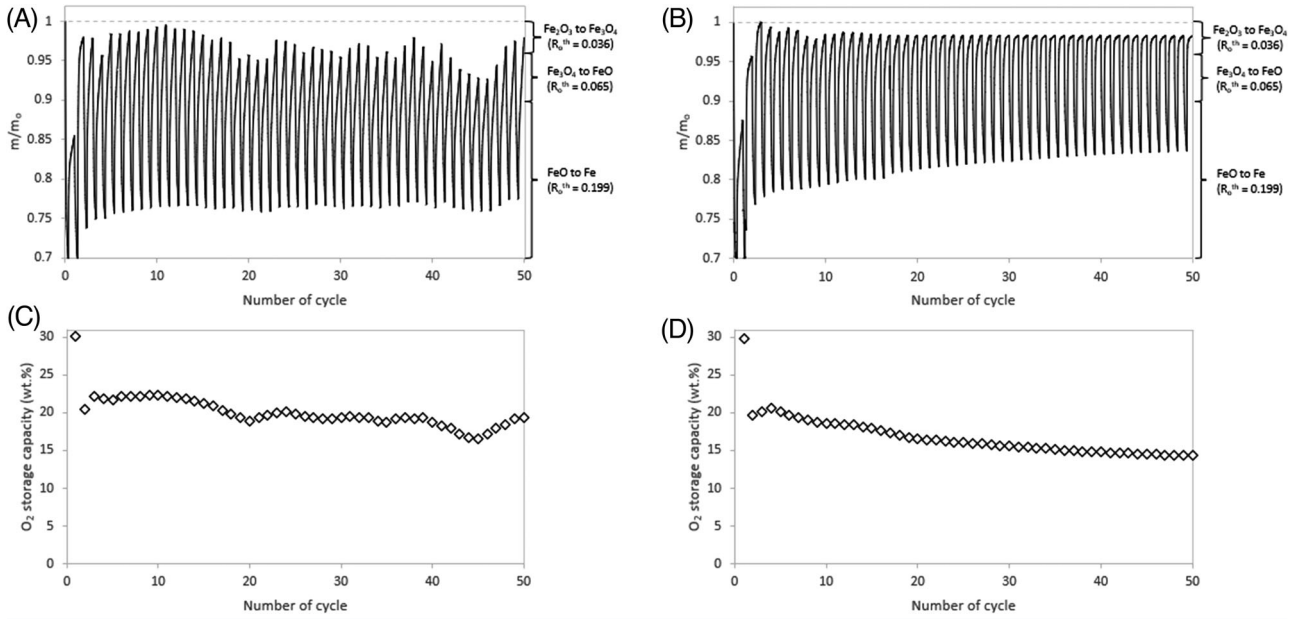

Figure 3. Results of the TGA experiments using the Fe_2O_3 reference samples as oxygen carrier over fifty redox cycles at 850°C: (A) The relative weight change, m/m_o, recorded during the redox cycling experiment, and (C) Ro for the Fe_2O_3-MM and (B) The relative weight change, m/m_o, recorded during the redox-cycling experiment, and (D) Ro for the Fe_2O_3-CP. The values for Ro^{th} represent the theoretical weight change for each phase transition change of iron oxide: transition from Fe_2O_3 to Fe_3O_4 has an $Ro^{th} = 0.036$, the next transition from Fe_3O_4 to FeO has an $Ro^{th} = 0.065$ and the final transition from FeO to Fe has an $Ro^{th} = 0.199$.

value of $m/m_o = 1$ in any of the samples in the first oxidation cycle (which would have meant full oxidation back to Fe_2O_3), and this was only achieved in cycle 3 for the Fe_2O_3-CP sample. The Fe_2O_3-MM sample did not reach full oxidation to Fe_2O_3 during the whole experiment. The relative weight change profile of the Fe_2O_3-MM samples shows and erratic behaviour, with oxidation after each cycle stopping at different m/m_o values and not reaching oxidation back to Fe_2O_3 in at least 15 cycles, which means that the oxidation only reached Fe_3O_4 in 30% of the experimental runs. The experimental value of the Ro measured for the Fe_2O_3-MM sample followed this same erratic trend and showed an overall decrease with cycling (Fig. 3C).

The value of Ro measured for the Fe_2O_3-CP sample decreased steadily after the 3rd cycle with continuous cycling, as can be seen in (Fig. 3D), reaching a final value of 14.5 wt.%. The oxidation step in the experiment appears to stabilise after 15 cycles and stopping at a value of $m/m_o = 0.98$ continuously until the end of the run. These results for both reference samples might suggest that sintering of the pores worsens with continuous cycling. Therefore, the surface morphology of the particles was studied. Results of the SEM analysis for the reference samples is shown in Fig. 4.

SEM images for both reference fresh samples show a dense particle with small grains in the surface of the particles of the Fe_2O_3-MM (Fig. 4A and B) and the Fe_2O_3-CP (Fig. 4C and D). The recovered oxygen carrier samples after redox-cycling exhibited sintering of the particles after the experiment, for both the Fe_2O_3-MM sample (Fig. 4E and F) and the Fe_2O_3-CP sample (Fig. 4G and H). A clear formation of a grain structure, in which the grains started to fuse within each other can be seen in (Fig. 4E and F). Less sintering within the grains can be observed for the Fe_2O_3-CP sample (Fig. 4G and H) compared to the Fe_2O_3-MM sample, but a fully developed grain structure within the surface of the Fe_2O_3-CP sample is observed. This sintering will result in an increase in the diffusion resistance through the surface of the particles, which results in the consistent decrease on the experimental Ro observed in (Fig. 3A and B).

Fe-W mixed oxides

The results of the experiments for the FeW-2-CP and FeW-5-CP samples are presented in Fig. 5 and 6,

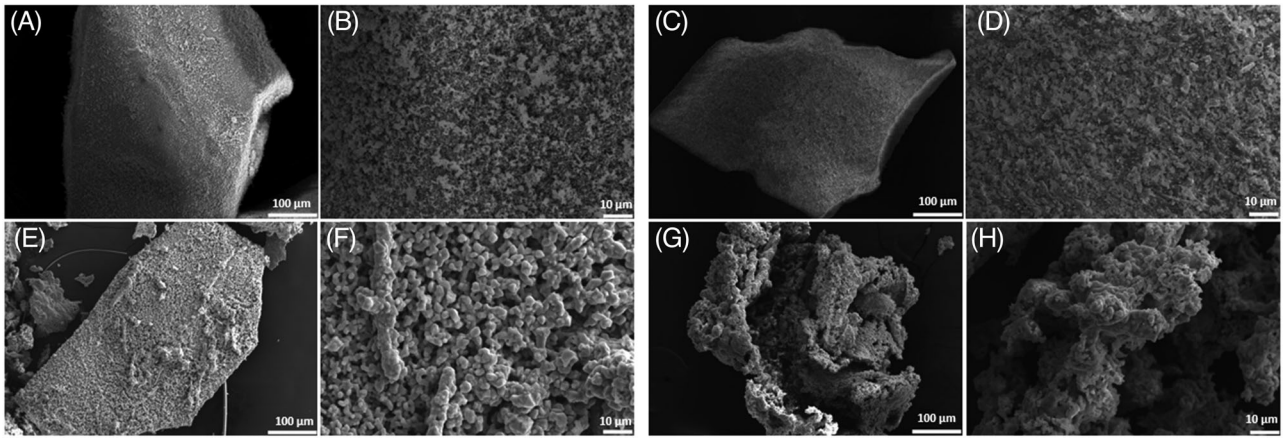

Figure 4. Scanning electron micrographs of fresh and cycled Fe_2O_3 reference samples. The micrographs show (A, B) the fresh Fe_2O_3-MM sample, (C, D) the fresh Fe_2O_3-CP sample, (E, F) the Fe_2O_3-MM sample after 50 cycles, and (G, H) the Fe_2O_3-CP sample after 50 cycles, SE micrographs with (A, C, E, G) ×200, and (B, D, F, H) ×1200 magnification.

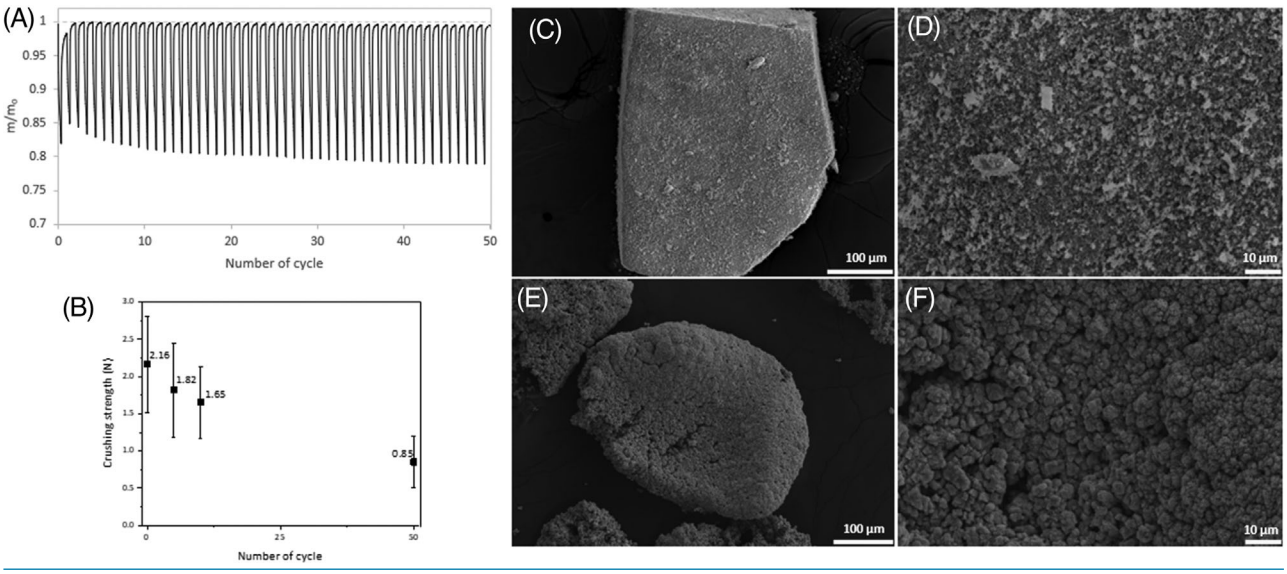

Figure 5. Results of the TGA experiments using the FeW-2-CP sample as oxygen carrier over 50 redox cycles at 850°C. (A) The relative weight change, m/m_o, recorded during the redox cycling experiment, (B) the crushing strength against cycle number, SEM images of (C, D) the fresh sample, and (E, F) the sample after 50 cycles, SE micrographs with (C, E) ×200, and (D, F) ×1200 magnification.

respectively. The relative weight change of the FeW-2-CP sample (Fig. 5A) showed a stable redox-cycling capability and a measured Ro of 19 wt.% during the last 20 cycles of the experiment. (Fig. 6A) shows an analysis on the relative weight change of the FeW-5-CP sample. The measured Ro increased during the experiment, with a maximum value of 17 wt.% at the end of the experiment. Both samples prepared using tungsten showed full reoxidation back to a value of $m/m_o = 1$ during continuous cycling, representing a significant improvement from the reference Fe_2O_3 samples.

The crushing strength of both samples decreased after the experimental run, most likely due to an increased porosity developed after cycling. The crushing strength of the FeW-2-CP (Fig. 5B) and the FeW-5-CP (Fig. 6B) decreased to 40% and 52% of their initial values, respectively. SE micrographs of the particles recovered after cycling showed the formation of a grain structure in the surface of the FeW-2-CP

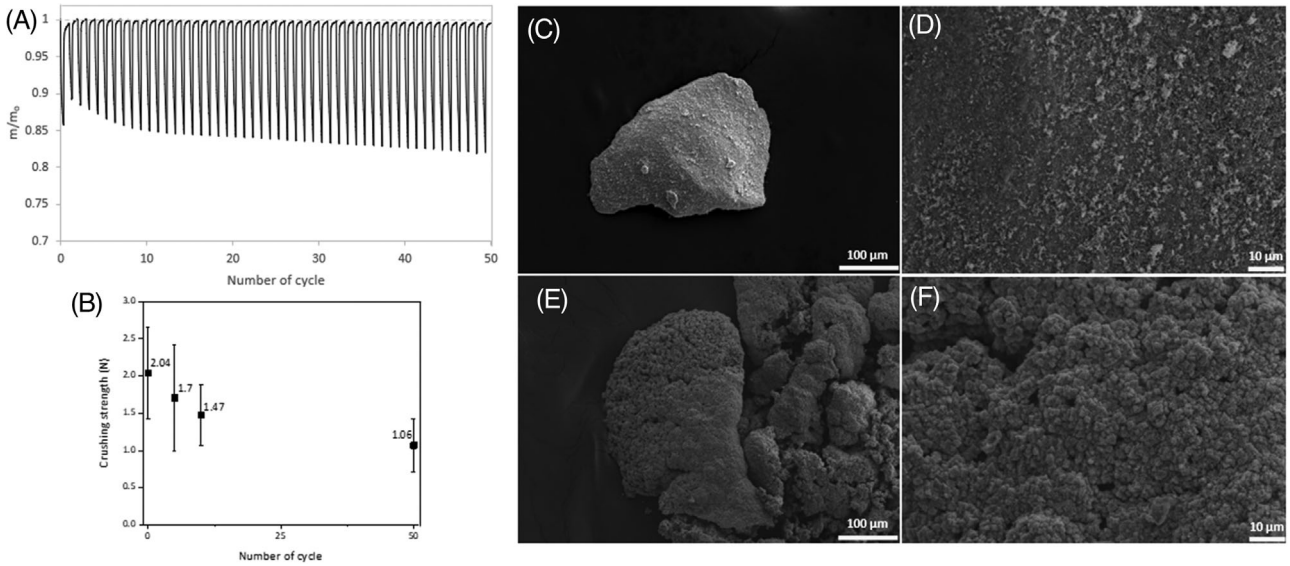

Figure 6. Results of the TGA experiments using the FeW-5-CP sample as oxygen carrier over 50 redox cycles at 850°C. (A) The relative weight change, m/m_o, recorded during the redox cycling experiment, (B) the crushing strength against cycle number, SEM images of (C, D) the fresh sample, and (E, F) the sample after 50 cycles, SE micrographs with (C, E) ×200, and (D, F) ×1200 magnification.

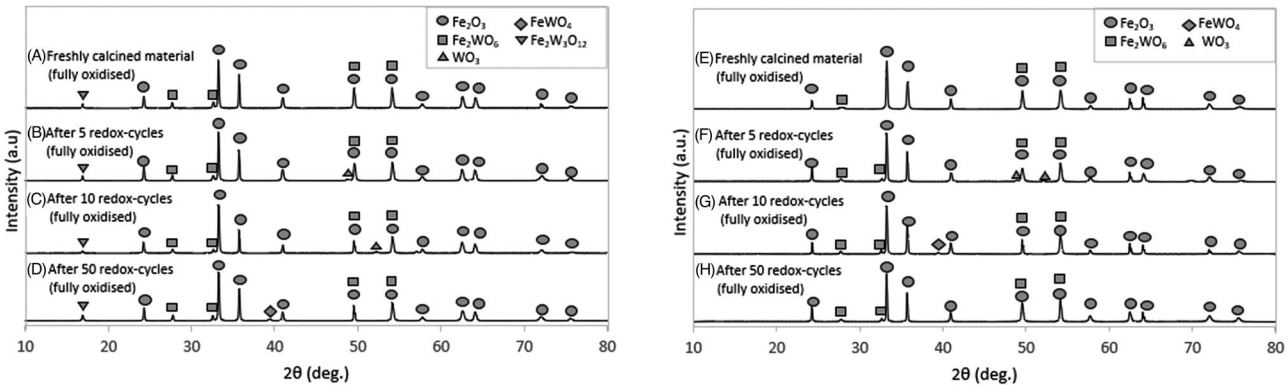

Figure 7. XRD plot of the FeW-5-CP sample in its fully oxidised state (A) before cycling, (B) after 5 redox cycles, (C) after 10 redox cycles, and (D) after 50 redox cycles, as well as the XRD plot of the FeW-2-CP sample in its fully oxidised state (E) before cycling, (F) after 5 redox cycles, (G) after 10 redox cycles, and (H) after 50 redox cycles.

(Fig. 5E and F) and the FeW-5-CP (Fig. 6E and F). The recovered particles showed no sign of agglomeration and some mild intraparticle sintering at the surface can be observed in Figs. (5F) and (6F) for both samples.

The X-ray diffraction analysis of the Fe-W samples (Fig. 7) was performed to study the change of the oxidised phases during cycling. XRD analysis confirmed that the major phase identified in all samples in the study is Fe_2O_3 (JCPDS 04-008-7627). The analysis showed the formation of different iron-tungstates structures: Fe_2WO_6 (JCPDS 00-042-0492), $FeWO_4$ (JCPDS 01-071-2390) and $Fe_2W_3O_{12}$ (JCPDS 00-024-0538), as well as WO_3 (JCPDS 04-007-2426). These previous results are in agreement with previous findings from Maiti et al.,[14] which found that the reduction and oxidation of the iron tungstate (Fe_2WO_6) goes through a series of intermediary phases. In the XRD patterns of the FeW-2-CP samples (Fig. 7E–H), the formation of $Fe_2W_3O_{12}$ was not identified, whereas it was formed in all the FeW-5-CP samples analysed (Fig. 7A–D). This was most likely because of the increased W available to form the intermediary phases. An analysis of the phase evolution of the W present in the FeW-2-CP during cycling showed an evolution to form the phase Fe_2WO_6, which appears to be the more stable form of

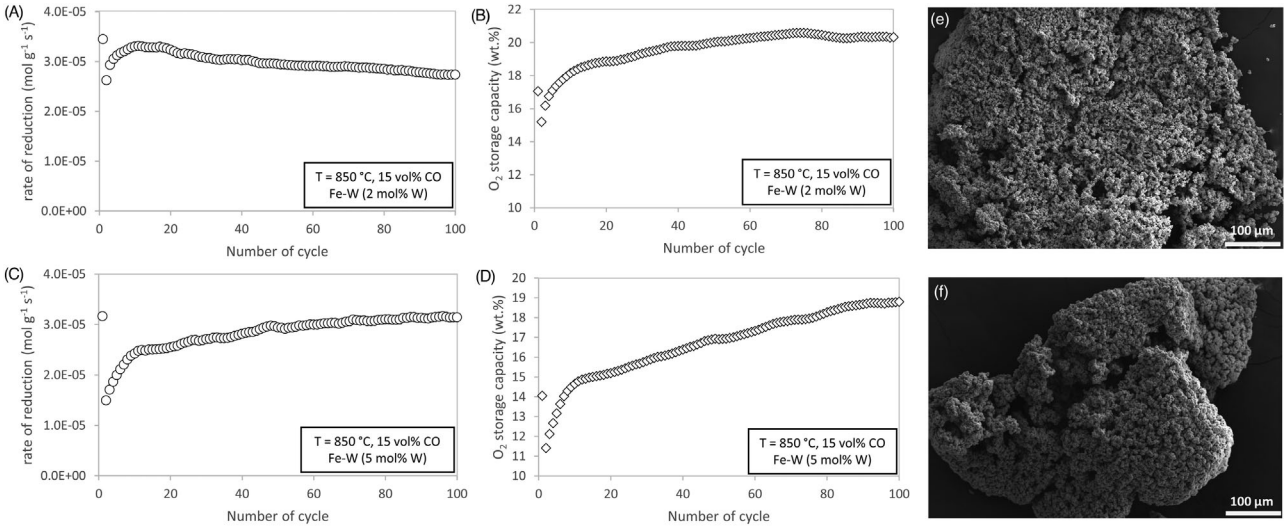

Figure 8. The maximum observed rate of reduction and Ro measured in the TGA at 850 C over 100 redox cycles using 15 vol% CO + N_2 for the reduction and 4 vol% O_2 for the oxidation: (A) observed rate and (B) Ro for the FeW-2-CP oxygen carrier and (C) observed rate and (D) Ro for the FeW-5-CP oxygen carrier, and SEM images of an oxygen carrier particle recovered after 100 redox cycles of the (E) FeW-2-CP and (F) FeW-5-CP, SE micrographs with (E, F) ×200 magnification.

the W present in the material. This phase became less apparent as the number of redox-cycles increase, most likely because the tungsten had formed a solid solution within the Fe_2O_3 matrix in the material.

Long-term redox cycling performance of the Fe-W OCs with CO

Long-term TGA experiments with CO were carried out to assess the CLC performance of the Fe-W oxygen carriers over 100 cycles. The samples were reduced in 15 vol% CO + N_2 for 10 min and oxidised in 4 vol% O_2 + N_2 for 20 min. The maximum observed rates of CO consumption and oxygen storage capacity of the materials are presented in Fig. 8.

(Figure 8A) shows that the maximum rate observed for the FeW-2-CP decreased from its initial value of 3.45×10^{-5} mol•g^{-1}•s^{-1} and quickly recovered over within the first 10 cycles, reaching a reactivity of almost the same value it had initially. The observed rate of reduction started to decrease steadily after cycle 20, from 3.25×10^{-5} mol•g^{-1}•s^{-1} to 2.75×10^{-5} mol•g^{-1}•s^{-1} at the end of the 100 redox-cycles. (Fig. 8C) shows that the FeW-2-CP particle started to disintegrate after 100 redox-cycles. The micrograph also shows that a highly porous structure had formed. It is possible that this was enhanced by bulk diffusion of metal ions outwards from the particle centre, as has been observed before.[15]

The maximum observed rate for the FeW-5-CP decreased from its initial value of 3.15×10^{-5} mol•g^{-1}•s^{-1} and steadily recovered over the duration of the experiment, reaching again the initial reactivity in the last ten cycles (Fig. 8C). Similarly, (Fig. 8D) shows that the Ro for this material had a steady increase until reaching stability at the last ten cycles with an average value of 18.7 wt.%. The decrease and following recovery of the maximum rate of reduction was most likely to structural rearrangements, which then stabilize after around 100 cycles. (Fig. 8F) shows a FeW-5-CP particle recovered after 100 redox-cycles, which appears to have developed a highly porous structure while maintaining most of its integrity and shape. Given the additional cost of adding W to the system, and the apparent maximum in reactivity and Ro, it does not appear likely that adding additional W beyond 2 mol% is worthwhile.

Although an experiment testing 100 redox cycles may provide an indication of the long-term performance of the OCs, a much higher number of cycles would be required to estimate indicators such as lifetime of the particles.

Carbon deposition

Thermodynamically is possible that carbon was deposited on the iron oxide particles when reduction to

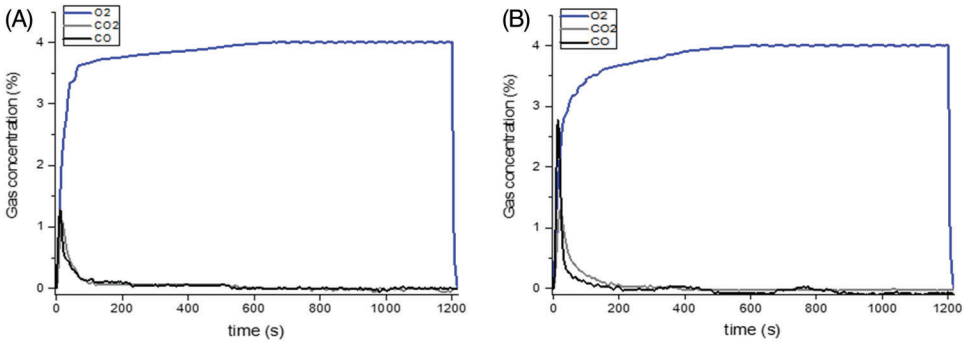

Figure 9. Concentration profile of the 5th oxidation cycle in the FBR cycling experiment at 850°C using 15 vol% CO + N_2 for the reduction and 4 vol% O_2 + N_2 for the oxidation: (A) Fe_2O_3-MM sample and (B) Fe_2O_3-CP sample. The gas flow rate was kept constant to maintain a value of u/u_{mf} of 3.

Fe was done with CO.[16] Since any residual carbon deposited on the surface of the particles would react with the oxygen to produce CO_2 and CO during the oxidation step, the extent of the carbon deposition was quantified from the deconvoluted CO_2 and CO gas concentration profiles measured during the oxidation step in the fluidised bed experiments (Fig. 9). CO_2 and CO produced was assumed to be formed via reactions 1 and 2, respectively.

$$C + O_2 \rightarrow CO_2 \qquad \text{(Reaction 1)}$$

$$2C + O_2 \rightarrow 2CO \qquad \text{(Reaction 2)}$$

Carbon deposition on the surface of the reference samples accounted for 2.25 wt.% and 5.45 wt.% of the initial sample mass of OC for the Fe_2O_3-MM and Fe_2O_3-CP, respectively. No carbon deposition was observed in the experiments with the Fe-W materials under the same conditions, a significant improvement most likely due to the high degree of metal dispersion and the resulted higher surface area of the Fe-W mixed oxides that may have improved the thermal and chemical stability of the material, which has been observed before.[17–19] Of course, increasing the amount of CO_2 in the feed can also reduce the amount of carbon deposited.

Conclusions

This work demonstrated that the synthesis of Fe-W mixed oxides via co-precipitation to be used as oxygen carrier in CLWS as a promising option. The alloying of Fe with small amounts of W showed an improvement of the reactivity over continuous CLC operation. We have compared the performance of the mixed oxides with two reference sample materials (Fe_2O_3) and the Fe-W oxides showed no sign of agglomeration and a resistance to carbon deposition, whereas both reference materials showed carbon deposition and a decrease in the measured Ro, and redox capability that can be attributed to the observed sintering of the particles recovered after cycling.

The stable reactivity and performance of the new Fe-W OCs can be attributed to the formation of a solid solution between the iron oxide and the W in the material, which increases the melting point of the reduced phases of the material, therefore avoiding sintering and agglomeration problems. The results of the XRD analysis suggest that the W present in the material goes through different intermediary phases during redox-cycling. Further analysis should focus on the phase evolution of the Fe-W mixed oxide to determine the influence of the transition phases during the first few redox cycles and the later stabilisation of the OC performance. Further studies with lower W content could further explain how the stabilisation of the Ro and reaction rate is influenced by the intermediary iron-tungstate phases.

Acknowledgements

JJMC would like to thank Conacyt-SENER for the funding of his PhD scholarship (No. 2018-000061-02EXTF-00046), and PhD student Shaoqing Qu for conducting the XRD analysis at the University of Sheffield facilities. KSC would like to thank the Royal Society and EPSRC for her Dorothy Hodgkin Research Fellowship (Dhf150014).

References

1. IEA. Greenhouse gas emissions from energy: overview. Paris, France; IEA: 2021. https://www.iea.org/reports/greenhouse-gas-emissions-from-energy-overview
2. Bui, M., Adjiman CS, Bardow A, Anthony EJ, Boston A, Brown S, et al. Carbon capture and storage (CCS): the way forward. Energy Environ Sci. 2018;11(5):1062–76.
3. IEA. CO_2 capture and storage: A key carbon abatement, Paris, France; IEA: 2008. https://www.iea.org/reports/co2-capture-and-storage-a-key-carbon-abatement-option
4. Soltani R, Rosen MA, Dincer I. Assessment of CO_2 capture options from various points in steam methane reforming for hydrogen production. Int J Hydrogen Energy. 2014;39(35):20266–75.
5. Tong A, Sridhar D, Sun ZC, Kim HR, Zeng L, Wang F, et al. Continuous high purity hydrogen generation from syngas chemical looping 25 kW(th) sub-pilot unit with 100% carbon capture. Fuel. 2013;103:495–505.
6. Kang K-S, Kim C-H, Bae K-K, Cho W-C, Kim S-H, Park C-S. Oxygen-carrier selection and thermal analysis of the chemical-looping process for hydrogen production. Int J Hydrogen Energy. 2010;35(22):12246–54.
7. Yu Z, Yang Y, Yang S, Zhang Q, Zhao J, Fang Y. et al. Iron-based oxygen carriers in chemical looping conversions: a review. Carbon Resour Convers. 2019;2:23–34.
8. Boot-Handford ME, Abanades JC, Anthony EJ, Blunt MJ, Brandani S, Mac Dowell N, et al. Carbon capture and storage update. Energy Environ Sci. 2014;7:130–89.
9. Jerndal E, Mattison T, Lyngfelt A. Thermal analysis of chemical-looping combustion. Chem Eng Res Des. 2006;84(9):795–806.
10. Bleeker MF, Veringa HJ, Kersten SRA. Deactivation of iron oxide used in the steam-iron process to produce hydrogen. Appl Catal, A. 2009;357:5–17.
11. Patzschke CF, Boot-Handford ME, Song Q, Fennell PS. Co-precipitated Cu-Mn mixed metal oxides as oxygen carriers for chemical looping processes. Chem Eng J. 2021;407:127093.
12. Zhang Z, Hills TP, Scott SA, Fennell PS. Spouted bed reactor for kinetic measurements of reduction of Fe_2O_3 in a CO_2/CO atmosphere Part I: Atmospheric pressure measurements and equipment commissioning. Chem Eng Res Des. 2016;114:307–20.
13. Fennell PS, Pacciani R, Dennis JS, Davidson JF, Hayhurst AN. The effects of repeated cycles of calcination and carbonation on a variety of different limestones, as measured in a hot fluidized bed of sand. Energy Fuels. 2007;21:2072–81.
14. Maiti GC, Löchner U, Baerns M. Studies on the Reduction of iron/tungsten mixed oxides. Thermochimica. 1987;112:221–9.
15. Li F, Sun Z, Luo S, Fan LS. Ionic diffusion in the oxidation of iron-effect of support and its implications to chemical looping applications. Energy Environ Sci. 2011;4:876–80.
16. Bohn CD, Scott SA, Müller CR, Cleeton JP, Hayhurst JF, Davidson JF, Dennis, JS. Production of very pure hydrogen with simultaneous capture of carbon dioxide using the redox reactions of Iron oxides in packed beds. Ind Eng Chem Res. 2008;47(20):7623–30.
17. Charisiou ND, Siakavelas G, Papageridis KN, Baklavaridis A, Tzounis L, Goula G, et al. The effect of WO_3 modification of ZrO_2 support on the Ni-catalyzed dry reforming of biogas reaction for syngas production. Front Environ Sci. 2017;5:66.
18. Bychkov VY, Tyulenin YP, Firsova AA, Shafranovsky EA, Gorenberg AY, Korchak VN. Carbonization of nickel catalysts and its effect on methane dry reforming. Appl Catal, A. 2013;453:71–9.
19. Charisiou ND, Douvartzides SL, Siakavelas GI, Tzounis L, Sebastian V, Stolojan V, et al. The relationship between reaction temperature and carbon deposition on nickel catalysts based on Al_2O_3, ZrO_2 or SiO_2 supports during the biogas dry reforming reaction. Catalysts. 2019;9:676.

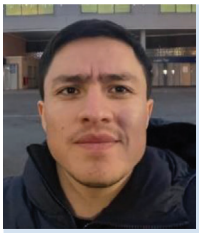

Jose Juan Morales Corona

Jose Juan Morales Corona is a PhD candidate in Chemical Engineering at Imperial College London. His research focuses on high-temperature looping cycles for CO_2 capture, focusing on material development, characterisation and testing.

Kyra L. Sedransk Campbell

Kyra L. Sedransk Campbell has a PhD in Chemical Engineering and a senior lecturer at the University of Sheffield working on materials degradation and decomposition. Her research operates at the interface of chemical engineering, materials science and chemistry studying the fundamentals that drive the changes that occur in dynamic, multiphase systems.

Paul S. Fennell

Paul S. Fennell has a PhD in Chemical Engineering and is a professor in the Department of Chemical Engineering at Imperial College London. His research focuses on clean production of energy and hydrogen, including hybrid processes for co-production of hydrogen and valuable materials (steel, cement, chemicals), integration of different industries to decarbonise them, among other related topics.